coupling theory with the localized wake force showed a strong head-tail instability, which has been seen in strong-strong beam-beam simulations.

2.3.5 References

1. K. Ohmi, proceedings of IPAC2016.
2. K. Ohmi, N. Kuroo, K. Oide, D. Zhou, F. Zimmermann, "Coherent beam-beam instability in collisions with a large crossing angle", Phys. Rev. Lett.,119, 134801 (2017).
3. A. W. Chao, "Physics of Collective Beam Instabilities in High Energy Accelerators", Wiley-Interscience Publication, New York, 1993).

2.4 FCC-ee Parameter Optimization

Dmitry Shatilov
Mail to: Shatilov@inp.nsk.su
BINP, Novosibirsk 630090, Russia

2.4.1 Introduction

FCC-ee is a double-ring e^+e^- collider which will work in the wide energy range from Z-pole (45.6 GeV) to ttbar (up to 185 GeV). At such high energies, beam-beam effects can get an extra dimension due to beamstrahlung (BS) – radiation in the field of the oncoming bunch [1, 2]. FCC-ee apparently will be the first collider where BS plays a significant role in the beam dynamics. For this to happen, two conditions must be fulfilled: high energy and high charge density in the bunches. For example, the energy in LEP was large enough, but the charge density too small, so the effect was negligible. BS increases the energy spread (and hence the bunch length) and creates long non-Gaussian tails in the energy distribution, that can limit the beam lifetime due to a possible ingress of particles beyond the energy acceptance.

Next, we will only consider the optimization process associated with the beam-beam effects. The actual table of parameters can be found in [3]. The collider has a two-fold symmetry and two IPs with a horizontal crossing angle and crab waist collision scheme [4, 5]. The luminosity per IP for flat beams ($\sigma_y << \sigma_x$) can be written as:

$$L = \frac{\gamma}{2er_e} \cdot \frac{I_{tot}\xi_y}{\beta_y^*} \cdot R_{hg}\,, \tag{1}$$

where I_{tot} is the total beam current which in our case is determined by the synchrotron radiation power 50 MW. Therefore L can be increased only by making ξ_y larger and β_y^* smaller while keeping R_{hg} reasonably large. We assume that ξ_y can be easily controlled by N_p (number of particles per bunch), that implies adjusting the number of bunches N_b to keep I_{tot} unchanged.

The hour-glass factor R_{hg} depends on L_i/β_y^* ratio, where L_i is the length of interaction area which in turn depends on σ_z and Piwinski angle ϕ:

$$\phi = \frac{\sigma_z}{\sigma_x} tg\left(\frac{\theta}{2}\right), \tag{2}$$

$$L_i = \frac{\sigma_z}{\sqrt{1+\phi^2}} \Rightarrow \frac{2\sigma_x}{\theta}. \tag{3}$$

Here θ is the full crossing angle, and expressions after arrow correspond to $\phi >> 1$ and $\theta << 1$, see Fig. 1.

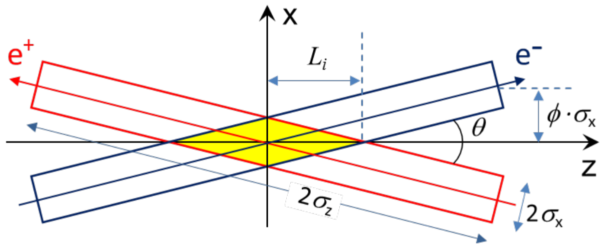

Figure 1: Collision scheme with large Piwinski angle.

The beam-beam parameters for $\sigma_y << \sigma_x$ and $\theta \neq 0$ become [6]:

$$\begin{aligned} \xi_x &= \frac{N_p r_e}{2\pi\gamma} \cdot \frac{\beta_x^*}{\sigma_x^2(1+\phi^2)} \Rightarrow \frac{N_p r_e}{\pi\gamma} \cdot \frac{2\beta_x^*}{(\sigma_z\theta)^2} \\ \xi_y &= \frac{N_p r_e}{2\pi\gamma} \cdot \frac{\beta_y^*}{\sigma_x\sigma_y\sqrt{1+\phi^2}} \Rightarrow \frac{N_p r_e}{\pi\gamma} \cdot \frac{1}{\sigma_z\theta}\sqrt{\frac{\beta_y^*}{\varepsilon_y}} \end{aligned} \tag{4}$$

In particular, $\xi_x \propto 1/\varepsilon_x$ (in head-on collision) transforms to $\xi_x \propto \beta_x^*/\sigma_z^2$ when $\phi >> 1$, and ξ_y dependence on σ_x vanishes. Further, because of the symmetry, we consider a model with one IP (that is a half ring of the real collider).

2.4.2 Luminosity Optimization at the Top Energy

At 175÷185 GeV the beam lifetime is determined mainly by single high-energy BS photons [2], that imposes another limitation on the luminosity. For the beamstrahlung lifetime we have [7]:

$$\tau_{BS} \propto \exp\left(\frac{2\alpha\eta\rho}{3r_e\gamma^2}\right) \cdot \frac{\rho\sqrt{\eta\rho}}{L_i\gamma^2}, \tag{5}$$

where α is a fine structure constant, η is the energy acceptance (which should be maximized), and ρ is the bending radius of particle's trajectory in the field of oncoming bunch. Evidently, ρ is inversely proportional to the absolute value of transverse electromagnetic force acting on the particle. Its dependence on the transverse coordinates for flat beams is shown in Fig. 2. The lifetime is determined by the minimum values of ρ which correspond to the particles with $|x| < \sigma_x/2$ and $|y| > 2\sigma_y$. However, during collision particles traverse the opposite bunch horizontally because of the crossing angle. This means that the maximum force depends mainly on the vertical coordinate, and ρ is inversely proportional to the surface charge density in the horizontal plane:

$$\frac{1}{\rho} \propto \frac{N_p}{\gamma\sigma_x\sigma_z} \propto \frac{\xi_y}{L_i}\sqrt{\frac{\varepsilon_y}{\beta_y^*}} \propto L\sqrt{\frac{\varepsilon_y}{\beta_y^*}}\,. \tag{6}$$

These relations are valid for both head-on and crossing angle collisions; the last transformation is based on (1) and assumption that $L_i \approx \beta_y^*$.

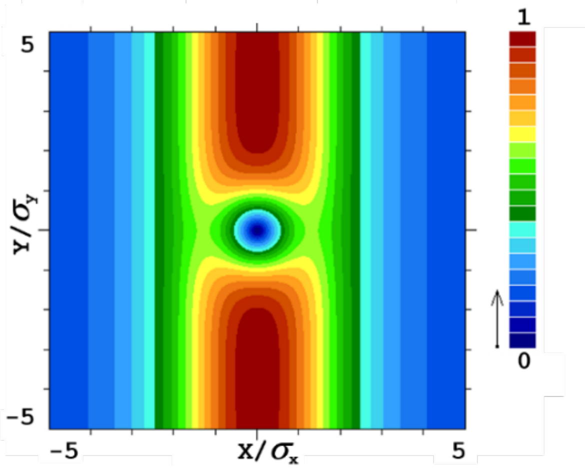

Figure 2: Absolute value of transverse force for flat beams, in relative units.

Our goal is to increase L while keeping the lifetime (and therefore ρ) large enough. It follows that ε_y (i.e. both the betatron coupling and ε_x) should be minimized, and β_y^* should be *increased*. For example, increase in β_y^* (together with L_i) by a factor of k may result in the luminosity gain by $k^{1/2}$ with ρ unchanged. In fact, as is seen from (5), τ_{BS} is inversely proportional to L_i provided that $\rho = const$. Therefore, to keep $\tau_{BS} = const$ when L_i is increased, we need to slightly increase ρ. However, τ_{BS} dependence on L_i is much weaker than the dependence on ρ (because the argument of *exp* is >> 1), so the gain in luminosity will be “almost” $k^{1/2}$. All these manipulations mean an increase in σ_x and N_p, but other than that, ξ_y will also rise by $k^{3/2}$. Consequently, we may perform such optimization only as long as ξ_y remains below the beam-beam limit.

This can be formulated in a different way. If there are multiple limiting factors, the maximum performance is achieved when all limits are reached simultaneously. In our case it means that β_y^* (together with L_i) should be adjusted in such a way that both τ_{BS} and ξ_y achieve their limits. This implies that if the balance shifts towards "limit by the BS lifetime" (e.g. decrease in η or increase in γ, ε_y), the luminosity optimization will require some increase in L_i (together with β_y^*), and vice versa. But we should not forget that the condition $L_i \approx \beta_y^*$ is not very strict.

If the bunch population is less than the nominal value, BS for the counter (strong) bunch weakens and its length decreases accordingly. Therefore, BS for the weak bunch becomes stronger and its lifetime decreases. Top-up injection can provide an asymmetry within ± 3%, while the lifetime should be ≥ 15 minutes. For safety margins, we chose the nominal N_p to get a lifetime of ~25 minutes for $N_p^w = 0.97 \cdot N_p$ and $N_p^s = 1.03 \cdot N_p$. Hereinafter the superscripts w and s mark the weak and the strong beams, respectively.

To find the optimum beta-functions we tested several options, and assume for now that η does not depend on β^*. The results for 182.5 GeV are presented in Table 1. As we see, a decrease in β_x^* requires smaller N_p in order to keep the lifetime unchanged. Accordingly increase in β_x^* helps to rise up the luminosity. Comparing the last two columns, note that the luminosity increases by only 10% when β_y^* halves; the reason is the hour-glass which is just optimal for the rightmost column. Then, taking into account that in fact dynamic aperture and energy acceptance are larger for relaxed β^*, the values in last column ($\beta_x^* = 100$ cm, $\beta_y^* = 2$ mm) should be considered closest to the optimal.

Table 1: Luminosity at 182.5 GeV for different β^*.

Parameter	**β_x^* = 50 cm**		**β_x^* = 100 cm**	
ε_x / ε_y [pm]	1450 / 2.9			
σ_z (SR / BS) [mm]	2.5 / 3.3			
η	0.025			
Asymmetry	± 3%			
τ_{BS} [min]	~25			
ϕ (with BS)	1.84		1.3	
L_i [mm]	1.6		2.0	
N_p [10^{11}]	2.1		2.8	
N_b	52		39	
β_y^* [mm]	1	2	1	2
L [10^{34} cm^{-2}c^{-1}]	1.5	1.3	1.65	1.5

2.4.3 Beam-Beam Interaction at Low Energies

When energy decreases, the lifetime limitation due to BS weakens. This is easy to understand from the following considerations. Assuming that the lattice is not changed, emittances drop quadratically and σ_x, L_i – linearly with energy. If we keep ξ_y and β_y^* unchanged then, as follows from (6) and (5), ρ remains constant and τ_{BS} grows significantly because its dependence on γ is very strong. Hence at low energies we may allow some reduction of η, and for higher luminosity we need to decrease β_y^* and ρ. Consequently, since the bending radius in dipoles remains unchanged, the relative contribution of BS to the energy spread grows and the bunch lengthening becomes larger. For example, σ_z increases due to BS almost 3.5 times at 45.6 GeV and only 1.3 times at 182.5 GeV. Why then we do not see this effect in low energy colliders? Because they have much higher magnetic field in the dipoles or, which is the same, much smaller bending radius in the arcs.

Reduction of β_y^* has also limitations related to its maximum value in the nearest to IP quadrupole QD0: β_y^{max} depends on L^* (distance from IP to the quad's edge) and its strength. If QD0 is divided longitudinally into several sections, as shown in Fig. 3, then at low energy we can use only the first section – with larger gradient. This moves the azimuth of β_y^{max} towards IP and helps to reduce β_y^*. In addition, the following sections can be turned in the opposite polarity and used as QF1.

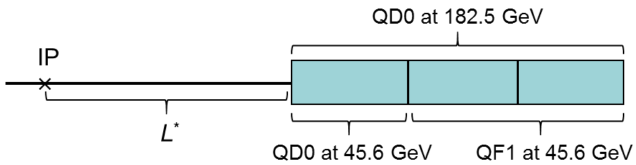

Figure 3: Longitudinal slicing of QD0.

Next we will consider the beam-beam effects at 45.6 GeV, where $\beta_y^* = 0.8$ mm can be obtained [3]. Decreasing σ_x and increasing σ_z leads to $\phi >> 1$, so we can take full advantage of crab waist collision scheme. On the other hand, in collisions with $\phi >> 1$ new phenomena were recently discovered in simulations: 3D flip-flop [8] and coherent X-Z instability [9, 10]. It is these effects that now limit the collider performance, and further optimization was aimed at finding such parameters with high luminosity at which these instabilities do not arise.

2.4.3.1 *3D Flip-flop*

Flip-flop instability is a well-known effect. For flat beams, where the perturbations occur mainly in the vertical direction, the same applies to flip-flop: it is actually 1D. In FCC-ee we have another kind of flip-flop, which is essentially 3D; beamstrahlung makes the difference. The threshold depends on asymmetry in population of colliding bunches, which causes a positive feedback in the following chain:

1) Asymmetry in the bunch currents leads to asymmetry in the bunch lengths (due to beamstrahlung).
2) In collisions with $\phi >> 1$, asymmetry in the bunch lengths enhances synchrotron modulation of the horizontal kick for a longer bunch, thus amplifying synchro-betatron resonances. In addition, ξ_x^w grows quadratically and ξ_y^w – linearly with decrease of σ_z^s, so the footprint expands and can cross more resonances. All this leads to increase in both emittances of the weak bunch (but mainly ε_x^w).
3) An increase in ε_x^w has two important consequences: a) weakening of BS for a strong bunch, which makes it shorter, and b) growth of ε_y^w due to the betatron coupling, which leads to asymmetry in the vertical beam sizes.
4) As follows from Fig. 2, the greatest BS is experienced by the particles with the vertical coordinates $|y^w| > 2\sigma_y^s$. When $\sigma_z^w > \sigma_z^s$, the number of particles in the weak bunch experiencing strong BS increases while the number of such particles in the strong bunch decreases. Thus, asymmetry in the vertical beam sizes leads to further increase of asymmetry in the bunch lengths.
5) Now we go back to point 2, and the loop is closed.

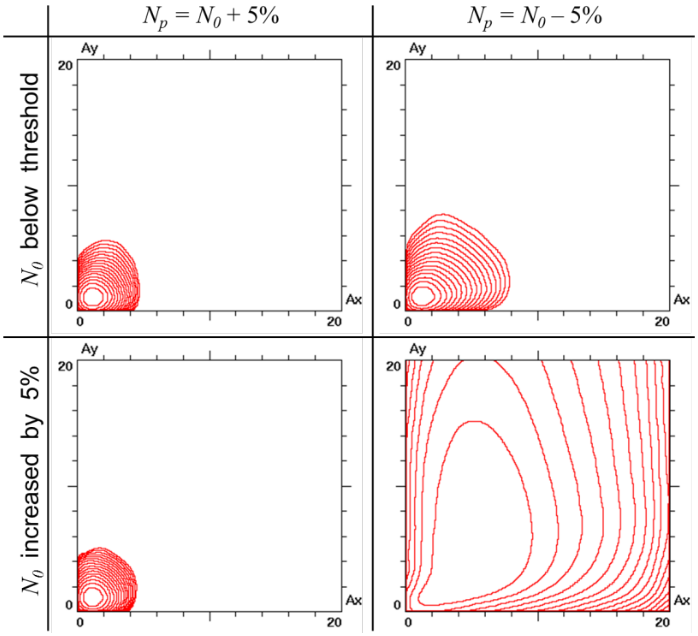

Figure 4: Example of 3D flip-flop. Density contour plots ($\sqrt{e}$ between successive lines) in the space of normalized betatron amplitudes are shown for stable (top) and unstable (bottom) cases.

In the end, we can get very strong blowups in all three directions, an example is shown in Fig. 4. Here asymmetry in the bunch currents is ± 5%. The top row corresponds to stable situation, though some acceptable blowup of the weak bunch is seen. In the bottom row asymmetry is the same, but N_p increased by 5%. As a result the strong bunch shrank to unperturbed sizes (as without beam-beam), while the weak bunch became swollen in all three dimensions. Hence, this instability can limit the maximum allowable N_p, and consequently the luminosity.

2.4.3.2 *Coherent X-Z instability*

This instability develops in the horizontal plane and it is manifested by wriggle of the bunch shape. If we imagine that the bunch is sliced longitudinally in many pieces, the amplitudes of X-displacement of the slices depend on their Z-coordinates and vary on every turn. In Fig. 5 we can see ε_x evolution with time and coordinates of centers of slices at different turns. Red line corresponds to unperturbed state, green – to oblique part of the curve on the right, and blue – to the final stage with ε_x blown up.

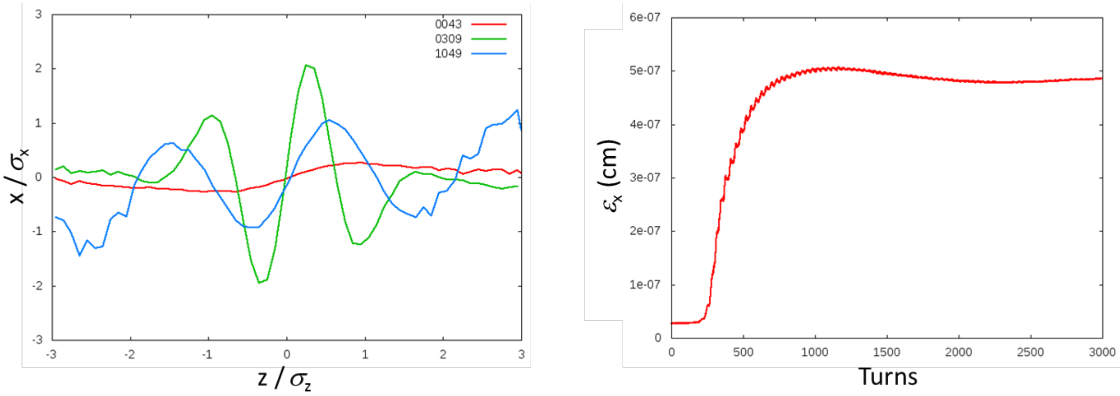

Figure 5: Example of coherent X-Z instability: the bunch shape at 43, 309 and 1049 turns (left) and evolution of the horizontal emittance (right).

The wriggles disrupt the operation of crab waist scheme, but the main damage is associated with a multiple increase in the horizontal emittance. In collision schemes with $\phi >> 1$, an increase in ε_x itself does not have a noticeable impact on luminosity. However, this leads to a proportional increase in ε_y due to the betatron coupling, so eventually the luminosity will decrease several times. The instability does not cause dipole oscillations and therefore cannot be suppressed by feedback. We need to look for conditions under which it does not arise.

2.4.3.3 *Parameters optimization at Z*

Both instabilities are associated with the growth of ε_x, therefore we have to reduce β_x^* which means a decrease in both the normalized horizontal kick and ξ_x. One of the features of FCC-ee IR design is the absence of local horizontal chromaticity correction sections. Because of this, β_x^* cannot be made too small, and attempts to do this lead to a decrease in the energy acceptance. Nevertheless, β_x^* can be reduced to 15 cm while obtaining a sufficient $\eta = 1.3\%$ [3]. Longitudinal slicing of QD0 and the use of its part as QF1 (see Fig. 3) helps to achieve this. However, this is not enough to suppress the instabilities.

The next step is to reduce ξ_x with a given β_x^*. In fact ξ_x is important not itself, but in comparison with ν_s. As we shall see later, the greatest danger arises from synchro-betatron resonances $2\nu_x - 2m\cdot\nu_s = 1$, the distance between them is just ν_s. Our task is to make ξ_x noticeably smaller than ν_s, then we can put the working point and the whole footprint between resonances. Herewith, by decreasing ξ_x we should preserve the luminosity, i.e. ξ_y. In assumption that $\beta_{x,y}^*$ and ε_y were already minimized and therefore are not free parameters, from (4) it follows that the only way to reduce ξ_x/ξ_y ratio is to increase the bunch length. The requirement of keeping ξ_y unchanged means that N_p/σ_z is constant, therefore ξ_x decreases by the same factor that σ_z grows (not quadratically as it may seem). However, if we simply reduce RF voltage, ν_s also decreases and the ratio ξ_x/ν_s does not change. We will return to lowering U_{RF} later, but now consider another way of the bunch lengthening: an increase in the momentum compaction factor α_p [11].

An advantage is that ν_s grows together (and by the same factor) with σ_z and $1/\xi_x$. In addition, larger α_p increases the threshold of microwave instability to an acceptable level. The main drawback of this approach is that ε_x also grows in the power of 3/2 with respect to α_p. As we already said, ε_x is not so important by itself, but ε_y should be small and it is usually proportional to ε_x, though at low energy some contribution to ε_y (0.2÷0.3 pm) comes from the detector solenoids. Besides, when the natural emittance is very small, various weak effects (feedback noises, etc.) become noticeable. For these and some other reasons, the lower limit for ε_y was set to 1 pm. Since the natural emittance at 45.6 GeV in the nominal lattice with small α_p is less than 90 pm, even its threefold increase still allows to obtain ε_y = 1 pm with adopted for FCC-ee betatron coupling 0.2%. Thus we switched to a lattice where doubling of α_p is achieved by reducing the phase advance per FODO cell in the arcs from 90°/90° to 60°/60° [3, 12]. At higher energies (80, 120 GeV), where instabilities are also present, this approach no longer has an advantage, due to an unacceptable increase in ε_y.

To select the working point, we performed a scan of betatron tunes in a simplified model: linear lattice without explicit betatron coupling. The beam-beam effects were implemented in a weak-strong approximation, so there are no coherent instabilities. The results are presented in Fig. 6.

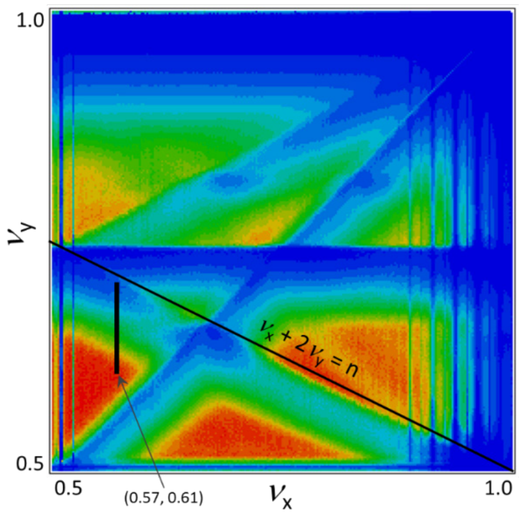

Figure 6: Luminosity as a function of betatron tunes. The color scale from zero (blue) to $2.3 \cdot 10^{36}$ cm^{-2}c^{-1} (red). The black narrow rectangle shows the footprint at (0.57, 0.61).

Since $\xi_x << \xi_y$, the footprint looks like a narrow vertical strip, bottom edge resting on the working point. Particles with small vertical betatron amplitudes have maximum tune shifts and are in the upper part of the footprint, so the resonances in Fig. 6 seem to be shifted down. The good region is reduced to a red triangle bounded by the main coupling resonance $\nu_x = \nu_y$, sextupole resonance $\nu_x + 2\nu_y = n$, and half-integer resonance $2\nu_x = 1$ with its synchrotron satellites. All other higher-order coupling resonances are suppressed by crab waist, and therefore are not visible. From this plot it is also clear that moving the working point to the right we should increase ν_y to keep the distance to the main coupling resonance. Both these actions lead to a decrease in the distance between the upper edge of the footprint and the resonance $\nu_x + 2\nu_y = n$. Thus, if we want to have large ξ_y, the range of permissible ν_x is bounded to the right by the values 0.57÷0.58.

Then we performed a scan of ν_x in a quasi-strong-strong model, in which coherent instabilities and flip-flop can be observed. The results are presented in Figures 7 and 8, where the synchro-betatron resonances are clearly seen. As the order of resonances increases their strength weakens, but we cannot move the working point too far to the right. Accordingly, for U_{RF} = 250 MV there are no regions free from coherent instability in the working range of ν_x. And here we are helped by the reduction of U_{RF}, thereby decreasing ν_s (while ξ_x / ν_s not changed) and increasing the order of resonances located in the region of interest. In the end, we can now find good working points. Note that N_p for the green lines in Figs. 7 and 8 was adjusted to get the same ξ_y as for the red line.

Here it is appropriate to recall the semi-analytical scaling law obtained from other considerations for the threshold bunch intensity [12]:

$$N_{th} \propto \frac{\alpha_p \sigma_\delta \sigma_z}{\beta_x^*}, \tag{7}$$

where σ_δ is the energy spread. In respect that $\alpha_p \sigma_\delta \propto \nu_s \sigma_z$ and $\xi_x \propto N_p \beta_x^* / \sigma_z^2$, this is nothing else than a condition on the ratio ξ_x / ν_s. We obtained a similar relation from the simple requirement to "squeeze" the footprint in between synchro-betatron resonances.

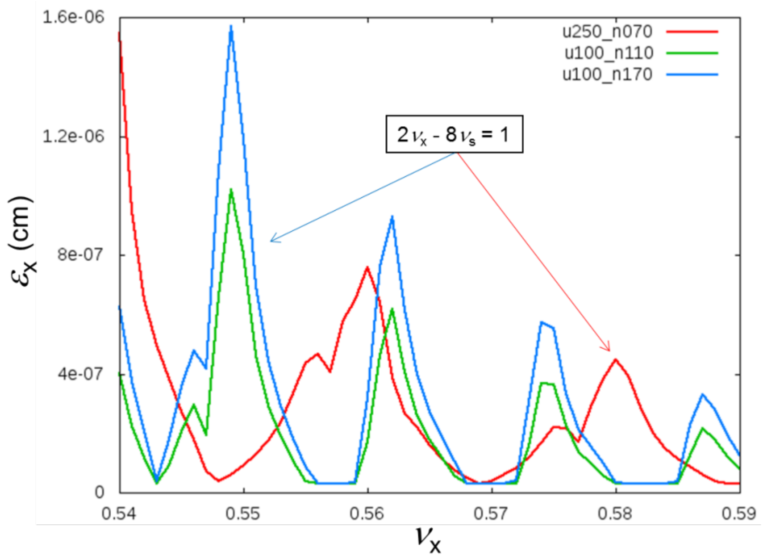

Figure 7: Growth of ε_x due to coherent X-Z instability, as a function of ν_x. Red line corresponds to U_{RF} = 250 MV, $N_p = 7{\cdot}10^{10}$, green and blue lines – U_{RF} = 100 MV, $N_p = 1.1{\cdot}10^{11}$ and $1.7{\cdot}10^{11}$.

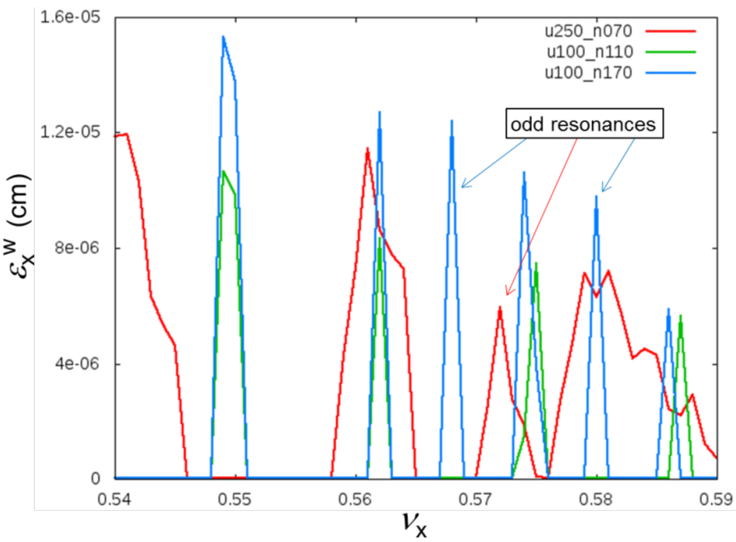

Figure 8: Growth of ε_x^w due to 3D flip-flop, as a function of ν_x. The colors are the same as in Fig. 7. Asymmetry in the bunch currents is ±5% for red and green lines, ±3% for blue line.

However, as for the threshold, it is not so simple. Indeed, as N_p increases, σ_z will also grow. In our range of parameters, where σ_z is defined mainly by BS, it scales as $\sigma_z^2 \propto N_p$. The rationale for this dependence is not so obvious, and we will not go into this, but in the simulation it was confirmed with good accuracy. As a result, it turns out that ξ_x does not depend on N_p. Thus if we stay in a good area, N_p can be increased – and there is simply no threshold. This is clearly seen in Fig. 7 comparing the green and blue lines, which differ only in N_p. The reverse side of this coin is that if we have instability, then getting rid of it simply by reducing N_p will be quite difficult. To do this, it is necessary to descend to the region where the dependence $\sigma_z^2 \propto N_p$ is violated, which means a decrease in the luminosity several times.

Then if we stay at a good point, what limits us? First, the increase in the energy spread (due to BS), which becomes comparable with that on the top energy. The non-Gaussian tails of the energy distribution are now not so long, but η has almost halved – as a result of a significant decrease in β_x^* and damping decrements. Consequently, as N_p grows, we will encounter a lifetime limitation by the energy acceptance. Secondly, by increasing ν_x (and correspondingly ν_y) we reduced the allowable ξ_y and approach the ordinary beam-beam limit. This is particularly evident in Fig. 8, where the asymmetry causes an additional increase in ξ_y^w which reinforces the flip-flop. And we see how additional odd resonances appear to the right – where the top of footprint approaches $\nu_x + 2\nu_y = n$. It means that minimizing asymmetry in the currents of colliding bunches again becomes critical.

In the end we can get high luminosity, but bunches will lengthen ~3.5 times because of BS. If we bring into collision so large currents with the "nominal" σ_z (energy spread created only by SR), the beam-beam parameters will be far above the limits and the beams will be blown up and killed on the transverse aperture, before they are stabilized by BS. To avoid this, we must gradually increase the bunch current during collision, so we come to bootstrapping. An example is presented in Fig. 9. We start with approximately one quarter of the final bunch population, then adding small portions to e^+ and e^- beams by turns. In fact, the injection cycle will last about 2 minutes, but in simulations it was reduced to ~2 damping times (10000 turns in "half-ring" collider).

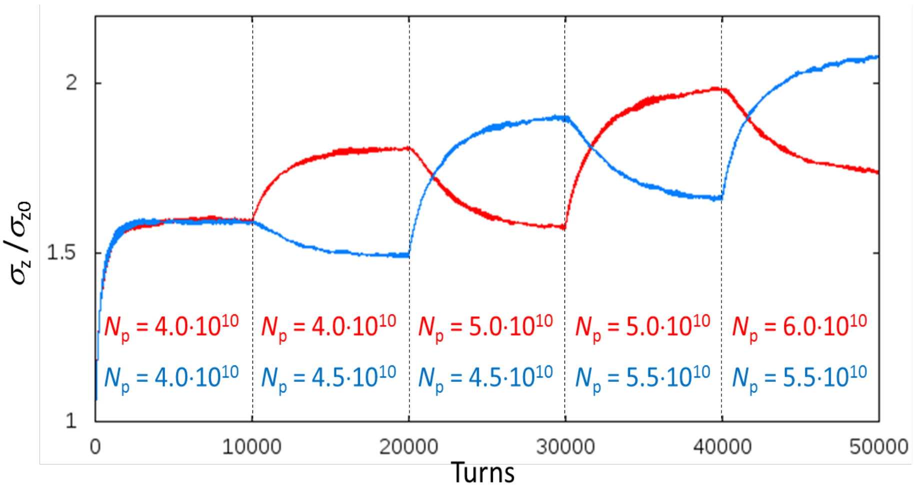

Figure 9: Simulated bootstrapping for Z-pole operation.

2.4.3.4 *Parameters optimization at W and HZ*

As the energy increases, the bunch lengthening and Piwinski angle decrease, while the damping decrements grow. Hereby both instabilities weaken, but still continue to be determining factors. In connection with this, the procedure for optimizing the parameters was similar to that at Z-pole and consisted of the following steps:

1) The RF voltage is made small, but so that RF acceptance still exceeds the energy acceptance, and this defines ν_s. Then ν_x is selected in the range of 0.565÷0.580 with a condition $\nu_x \approx 0.5 + \nu_s \cdot (m + 0.5)$, and $\nu_y = \nu_x + 0.03 \div 0.04$.
2) At this working point, we look for β_x^* at which the coherent X-Z instability disappears, while N_p is set to some reasonable value – as we said above, the threshold does not depend on this. The final value of β_x^* is selected slightly below the threshold (namely, 20 cm at 80 GeV and 30 cm at 120 GeV). In this case, the 3D flip-flop usually also disappears, and if not, just move ν_x a little.
3) The lattice optimization is performed for the selected β_x^* (and β_y^* = 1 mm) in order to maximize the dynamic aperture and energy acceptance [3]; hereby we obtain η (namely, 1.3% and 1.5%).
4) Then quasi-strong-strong simulations are performed with asymmetry ±3% (this is determined by the required beam lifetime and the injection cycle time). The bunch population N_p is scanned, while the restriction is the lifetime of the weak bunch. In this way, we determine the maximum N_p and luminosity.

Note that at 120 GeV single high-energy BS photons also become important, and they impose a limit on N_p, but β^* should be optimized from other considerations.

2.4.4 **Conclusion**

FCC-ee is designed for a wide range of energies, so the parameters optimization looks different at different points. The biggest problem at low energies is represented by two new phenomena found in simulations: 3D flip-flop and coherent X-Z instability. To combat them, the following steps were taken: an increase in the momentum compaction factor (at Z-peak only), a decrease in β_x^* and U_{RF} (and thereby in ν_s), an increase in $\nu_{x,y}$

by about 0.03 compared to the original design, and a neat choice of ν_x between synchro-betatron resonances. Note that an increase in $\nu_{x,y}$ has one more benefit: the tunes of the entire ring move farther from the integer, that facilitates the tuning of linear optics.

At the top energy, the instabilities are suppressed by very strong damping, but another problem becomes dominant: the lifetime limitation by single high-energy beamstrahlung photons. Therefore, in contrast to low energies, optimization requires an increase in beta-functions. It should also be noted that in the entire energy range, beamstrahlung plays a decisive role and luminosity is limited by the energy acceptance.

2.4.5 Acknowledgements

The author would like to thank K. Oide, K. Ohmi and M. Zobov for many useful discussions. This work has been supported by Russian Science Foundation (project N14-50-00080).

2.4.6 References

1. J. Augustin et al., “Limitations on Performance of e+e− Storage Rings and Linear Colliding Beam Systems at High Energy”, eConf C781015, 009 (1978).
2. V. Telnov, “Restriction on the Energy and Luminosity of e+e− Storage Rings due to Beamstrahlung”, Phys. Rev. Lett. 110, 114801 (2013).
3. K. Oide, “FCC-ee Optics Design”, in this Newsletter (2017).
4. P. Raimondi, D. Shatilov, and M. Zobov, “Beam-Beam Issues for Colliding Schemes with Large Piwinski Angle and Crabbed Waist”, LNF-07-003-IR (2007), e-Print: physics/0702033.
5. M. Zobov et al., "Test of Crab Waist Collisions at DAΦNE Phi Factory", Phys. Rev. Lett. 104, 174801 (2010).
6. P. Raimondi and M. Zobov, “Tune shift in beam-beam collisions with a crossing angle”, DAFNE Tech. Note G-58 (2003).
7. A. Bogomyagkov, E. Levichev and D. Shatilov, “Beam-beam effects investigation and parameters optimization for a circular e+e− collider at very high energies”, Phys. Rev. ST Accel. Beams, 17, 041004 (2014).
8. D. Shatilov, “Flip-flop Instability in FCC-ee at Low Energies”, presented at eeFACT2016, Daresbury, UK (2016).
9. K. Ohmi, “Study of Coherent Head-tail Instablility Due to Beam-beam Interaction in Cirular Colliders Based on Crab Waist Scheme”, in Proc. of eeFACT2016, Daresbury, UK (2016).
10. K. Ohmi, N. Kuroo et al., “Coherent Beam-Beam Instability in Collisions with a Large Crossing Angle”, Phys. Rev. Lett. 119, 134801 (2017).
11. D. Shatilov, “Simulation of X-Z Coherent Instability in FCC-ee @ 45.5 GeV Using Quasi-Strong-Strong Model”, 47th FCC-ee Optics Design Meeting, February 24 (2017), https://indico.cern.ch/event/615842/.
12. K. Oide et al., “Progress in the Design of Beam Optics for FCC-ee Collider Ring”, in Proc. of IPAC2017, Copenhagen, Denmark (2017).